Supplemental material

Reda et al., https://doi.org/10.1085/jgp.201812183

Determination of MHC composition, phosphorylation status, and stoichiometry of sarcomeric proteins in young and adult guinea pigs

Guinea pig ventricular tissue was finely pulverized in liquid nitrogen and solubilized using a muscle protein extraction buffer (2.5% SDS, 10% glycerol, 50 mM Tris base [pH 6.8 at 4°C], 1 mM dithiothreitol, 4 mM benzamidine HCl, 1 mM PMSF, 1 µg/ml leupeptin, and 1 µg/ml pepstatin). The final concentrations of all samples were adjusted to 2 mg/ml using protein loading dye (125 mM Tris-HCl [pH 6.8], 20% glycerol, 2% SDS, 0.01% bromophenol blue, and 50 mM β-mercaptoethanol). For determining the MHC composition, equal amounts of protein were loaded on a large SDS gel (30% acrylamide: 0.3% bis-acrylamide). The stacking and separating gels were 5% and 6% acrylamide (wt/vol), respectively. The samples were run for 14 h at constant current of 30 mAMP at 4°C. The gel was fixed in a solution containing 40% methanol and 10% acetic acid for 30 min, stained in Bio-Safe Coomassie G-250 Stain (Bio-Rad Laboratories) for ∼1 h, and destained in Milli-Q water for ∼3 h. The gel was imaged on Bio-Rad ChemiDoc XRS camera to visualize the MHC band profiles. Relative MHC content was quantified by densitometric analysis using ImageJ software (National Institutes of Health, acquired from http://rsbweb.nih.gov/ij/). For assessing the phosphorylation status of various cardiac sarcomeric proteins, 10 µg of standardized (2 mg/ml) protein samples were loaded and run on a 12.5% small SDS gel. The gel was subsequently fixed in a solution containing 50% methanol and 10% acetic acid and then treated with Pro-Q diamond stain and destain (P33300 and P33310; Life Technologies), as described in the manufacturer's manual. Phospho-proteins were visualized by imaging the gel using UV transillumination on a Bio-Rad ChemiDoc XRS camera. Following Pro-Q visualization, the gel was stained using Coomassie brilliant blue (R-250; Bio-Rad Laboratories), destained using a solution containing 25% methanol, and reimaged to visualize the total amounts of various sarcomeric proteins.

Detergent-skinned guinea pig cardiac multicellular preparations

Guinea pigs were deeply anesthetized with isoflurane, and hearts were quickly excised and placed into an ice-cold high-relaxing solution (20 mM 2,3-butanedione monoxime, 50 mM *N,N*-bis (2-hydroxyethyl)-2-aminoethanesulfonic acid [BES; pH 7.0], 30.83 mM potassium propionate [K-prop], 10 mM NaN_3, 20 mM EGTA, 6.29 mM $MgCl_2$, 6.09 mM Na_2ATP, 1.0 mM DTT, 4 mM benzamidine-HCl, 5 µM bestatin, 2 µM E-64, 10 µM leupeptin, 1 µM pepstatin, and 200 µM PMSF). Left ventricular papillary muscle bundles were removed and dissected into muscle preparations that were 150–200 µm in thickness and 2–2.5 mm in length. Muscle preparations were then detergent skinned in high-relaxing solution containing 1% Triton-X-100 incubated overnight at 4°C.

Composition of pCa solutions

The compositions of pCa solutions were calculated based on the program by Fabiato and Fabiato (1979). Two stocks of pCa solutions were first made: pCa 4.3 (50 mM BES, 5 mM NaN_3, 10 mM phosphoenol pyruvate (PEP), 10 mM EGTA, 10.11 mM $CaCl_2$, 6.61 mM $MgCl_2$, 5.95 mM Na_2ATP, and 31 mM K-Prop) and pCa 9.0 (50 mM BES, 5 mM NaN_3, 10 mM PEP, 10 mM EGTA, 0.024 mM $CaCl_2$, 6.87 mM $MgCl_2$, 5.83 mM Na_2ATP, and 51.14 mM K-Prop). All intermediate pCa solutions were made by mixing appropriate amounts of pCa 4.3 and pCa 9.0 solutions (Fabiato and Fabiato, 1979). The pH and ionic strength of all pCa solutions were adjusted to 7.0 and 180 mM, respectively.

Measurement of ATPase activity

Steady state isometric ATPase activity was measured using an enzymatically coupled assay, as previously described (de Tombe and Stienen, 1995; Stienen et al., 1995; Chandra et al., 2005). A beam of near-UV light was projected through the muscle chamber, then split equally (50:50) via a beam splitter and detected at 340 nm and at 400 nm. Because light intensity of the beam at 340 nm is sensitive to changes in NADH, a change in the UV absorbance at 340 nm could be linearly correlated to the oxidation of NADH (i.e., ATP usage) through enzymatically coupled reactions as follows: pyruvate kinase converts PEP and the ADP generated from steady state ATP hydrolysis of actin–myosin complex to ATP and pyruvate. Pyruvate is subsequently converted to lactate by lactate dehydrogenase in a reaction that is coupled to the oxidation of NADH to NAD^+. Light intensity of the beam at 400 nm is insensitive to changes in NADH and served as the reference signal. After each recording, the UV absorbance signal of NADH was calibrated by multiple rapid injections of 25 pmol of ADP into the bathing solution, with a motor-controlled calibration pipette.

Measurement of contractile dynamic parameters

A family of various amplitude quick stretches/releases (±0.5, ±1.0, ±1.5, and ±2.0% of the initial ML) was imposed on muscle preparations in the steady state of maximal Ca^{2+} activation (pCa 4.3), and the corresponding force responses were recorded, as previously described (Ford et al., 2010). An NLRD model was fitted to this family of force responses to estimate five NLRD model parameters: the magnitude of instantaneous increase in force caused by a sudden change in ML (E_D); the rate by which force dissipates due to detachment of strongly bound XBs (c); the nonlinear interaction parameter representing the negative impact of strained XBs on other

force-bearing XBs (γ); the rate of delayed force rise as XBs are recruited into the force-bearing state at the increased ML (b); and the magnitude of ML-mediated increase in steady state force due to recruitment of additional force-bearing XBs (E_R). The characteristic features of ML-mediated force responses and the physiological significance of the NLRD model parameters are described below. Fig. S1 shows a length protocol of 2% sudden stretch (Fig. S1 A) and the corresponding force response (Fig. S1 B) from a representative muscle preparation.

E_D

A sudden increase in ML (Fig. S1 A) causes an instantaneous increase in force from the isometric steady state value (F_{ss}) to F_1 (Fig. S1 B; phase 1). F_1 results from the distortion of the elastic elements within strongly bound XBs; thus, F_1 is proportional to the number of strongly bound XBs in the steady state prior to ML change. E_D is estimated as the slope of the relationship between changes in F_1–F_{ss} and the imposed changes in ML (ΔL) and thus provides an approximate measure of the number of strongly bound XBs (Campbell et al., 2004; Ford et al., 2010).

c

As the muscle is held at the increased ML (Fig. S1 A), force rapidly decays due to the detachment of XBs at a characteristic rate, c (Fig. S1 B; phase 2). Thus, c provides an approximate measure of XB detachment rate, g (Campbell et al., 2004).

γ

γ represents the negative effect of strained XBs on other force-bearing XBs. When the negative effect of strained XBs on other force-bearing XBs is less pronounced, force declines to a lesser extent (less prominent nadir), and γ is lower. In this regard, changes in γ can be coupled to allosteric/cooperative properties that exist within the myofilament. For instance, greater cooperativity at long SL attenuates the negative effect of strained XBs on other force-bearing XBs, leading to lower decline in force and lower γ.

b

As the muscle is maintained at the increased ML (Fig. S1 A), force begins to rise gradually at a characteristic rate, b (Fig. S1 B; phase 3), due to the recruitment of XBs into the force-bearing state.

E_R

At the increased ML, force eventually levels off to a new steady state value (F_{nss}) that is higher than F_{ss} (Fig. S1 B). Thus, the magnitude of increase in force, from F_{ss} to F_{nss}, is proportional to the number of additional force-bearing XBs recruited for the given increase in ML. Parameter E_R is derived as the slope of the relationship between changes in F_{nss}–F_{ss} and ΔL and thus represents the magnitude of ML-mediated increase in XB recruitment.

Rate constant of tension redevelopment (k_{tr})

k_{tr} was estimated using a modified version of the large slack/restretch maneuver originally designed by Brenner and Eisenberg (1986) and is described in our earlier published works (Ford et al., 2012; Gollapudi et al., 2012). During steady state maximal Ca^{2+} activation (pCa 4.3), muscle preparations were rapidly slackened by 10% of the initial ML using a servo motor and were briefly (25 ms) held at the decreased length. Muscle preparations were then lengthened by 10% past initial ML to detach any residual strongly bound XBs. Muscle preparations were then rapidly (0.5 ms) brought back to initial ML and allowed to redevelop force as detached XBs equilibrated into the force-bearing state. k_{tr} was estimated by fitting a monoexponential function to the rising phase of the force response,

$$F = (F_{ss} - F_{res})(1 - e^{-k_{tr}t}) + F_{res},$$

where F_{ss} is the steady state isometric force and F_{res} is the residual force from which the muscle preparation starts to redevelop force.

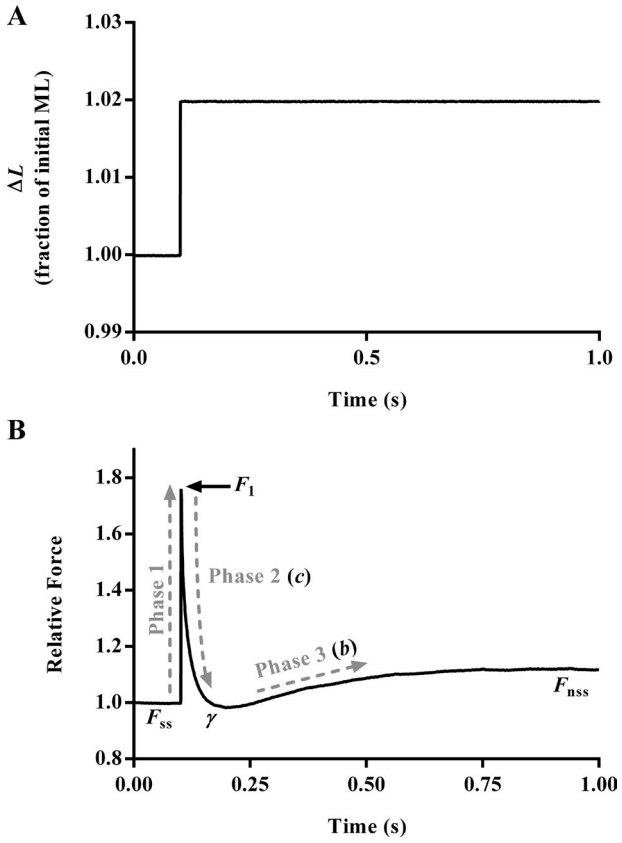

Figure S1. **Representative force response to a sudden 2% stretch. (A)** Representative 2% sudden stretch in ML imposed on a guinea pig cardiac muscle preparation at maximal Ca^{2+} activation (pCa 4.3). **(B)** The corresponding force response normalized to the isometric steady state force (F_{ss}) before ML change. The NLRD model was fitted to a family of force responses to step-like perturbations in ML (±0.5, ±1.0, ±1.5, and ±2.0% of initial ML) to estimate various model parameters (Ford et al., 2010). Dashed lines represent the different phases from which model parameters were estimated. F_1, the instantaneous increase in force due to sudden increase in ML (phase 1); *c*, the rate by which force decays following a sudden stretch in ML (phase 2); *γ*, nonlinear interaction term representing the negative impact of strained XBs on other force-bearing XBs; *b*, the rate of delayed force rise following an increase in ML (phase 3); and F_{nss}, the new steady state force corresponding to an increase in ML.

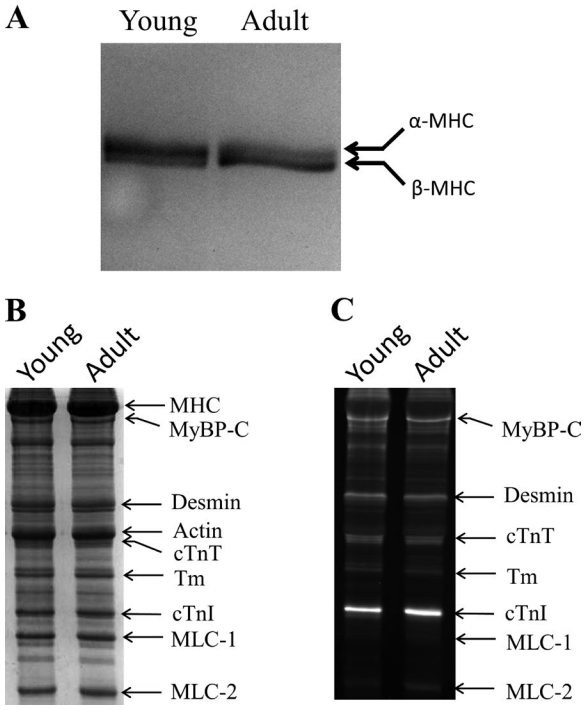

Figure S2. **SDS-PAGE and Pro-Q Diamond phospho analysis.** Ventricular muscle samples from young and adult guinea pig hearts were solubilized in 2.5% SDS solution and loaded on a large 6% SDS gel to determine the MHC composition. For determining the phosphorylation status and stoichiometry of sarcomeric proteins, protein samples were loaded and run on a small 12.5% SDS gel to separate various sarcomeric proteins. Pro-Q phospho staining of the gel was performed as described in the Life Technologies manual, and the gel was imaged to visualize the phosphorylation levels of various sarcomeric proteins. The gel was then stained with Coomassie brilliant blue and reimaged using a Bio-Rad ChemiDoc XRS camera (Life Technologies) to visualize the total expression of each sarcomeric protein. **(A)** Representative SDS gel showing the MHC composition in young and adult guinea pig hearts. Densitometric analysis showed that β-MHC expression was 20 ± 3% in young guinea pig hearts and 86 ± 4% in adult guinea pig hearts. Values reported as means ± SEM from three gels. **(B)** Coomassie blue–stained gel showing the total expression of each sarcomeric protein in young and adult guinea pig hearts. **(C)** Pro-Q Diamond–stained gel showing the phosphorylated levels of proteins in young and adult guinea pig hearts. MyBP-C, myosin binding protein C; cTnT, cardiac troponin T; Tm, tropomyosin; cTnI, cardiac troponin I; MLC-1, myosin light chain 1; and MLC-2, myosin light chain 2.

Table S1. **SL dependency of contractile parameters in young and adult guinea pig cardiac muscle preparations**

Parameter	Young			Adult		
	1.9 µm	2.3 µm	Δ	1.9 µm	2.3 µm	Δ
Maximal tension ($mN \cdot mm^{-2}$)	34.6 ± 1.3	48.8 ± 2.2***	↑41%	36.9 ± 0.7	51.5 ± 1.6***	↑39%
E_D ($mN \cdot mm^{-3}$)	803 ± 30	903 ± 43*	↑13%	764 ± 19	869 ± 22*	↑14%
pCa_{50}	5.64 ± 0.01	5.69 ± 0.01*	0.05	5.63 ± 0.01	5.74 ± 0.01***	0.11
n_H	2.52 ± 0.12	1.80 ± 0.07**	↓29%	3.00 ± 0.18	2.21 ± 0.12***	↓26%
c (s^{-1})	22.7 ± 1.72	15.7 ± 0.90***	↓31%	16.3 ± 1.29	6.56 ± 0.29***	↓60%
b (s^{-1})	7.18 ± 0.32	7.38 ± 0.45	↑3%	3.59 ± 0.11	4.05 ± 0.16	↑13%
γ (s^{-1})	41.9 ± 1.94	29.1 ± 1.23***	↓31%	30.8 ± 1.42	14.1 ± 0.97***	↓54%
E_R ($mN \cdot mm^{-3}$)	132 ± 5	236 ± 13***	↑79%	122 ± 6	304 ± 18***	↑149%
Tension cost ($pmol \cdot mN^{-1} \cdot mm^{-1} \times s^{-1}$)	4.76 ± 0.16	2.99 ± 0.13***	↓37%	3.12 ± 0.13	1.61 ± 0.09***	↓49%
k_{tr} (s^{-1})	4.30 ± 0.33	4.01 ± 0.29	↓7%	2.47 ± 0.19	1.67 ± 0.08	↓32%

Δ represents the change in contractile parameter in response to an increase in SL from 1.9 to 2.3 µm (↑ indicates increase, and ↓ indicates decrease). Significant differences were analyzed by two-way ANOVA and subsequent post hoc multiple comparisons (Holm–Sidak method). Asterisks indicate a significant difference when compared with data at SL 1.9 µm within each age group (*, $P < 0.05$; **, $P < 0.01$; and ***, $P < 0.001$). The number of preparations measured for all groups was 10. Data are expressed as means ± SEM.

References

Brenner, B., and E. Eisenberg. 1986. Rate of force generation in muscle: Correlation with actomyosin ATPase activity in solution. *Proc. Natl. Acad. Sci. USA.* 83:3542–3546. https://doi.org/10.1073/pnas.83.10.3542

Campbell, K.B., M. Chandra, R.D. Kirkpatrick, B.K. Slinker, and W.C. Hunter. 2004. Interpreting cardiac muscle force-length dynamics using a novel functional model. *Am. J. Physiol. Heart Circ. Physiol.* 286:H1535–H1545. https://doi.org/10.1152/ajpheart.01029.2003

Chandra, M., M.L. Tschirgi, and J.C. Tardiff. 2005. Increase in tension-dependent ATP consumption induced by cardiac troponin T mutation. *Am. J. Physiol. Heart Circ. Physiol.* 289:H2112–H2119. https://doi.org/10.1152/ajpheart.00571.2005

de Tombe, P.P., and G.J. Stienen. 1995. Protein kinase A does not alter economy of force maintenance in skinned rat cardiac trabeculae. *Circ. Res.* 76:734–741. https://doi.org/10.1161/01.RES.76.5.734

Fabiato, A., and F. Fabiato. 1979. Calculator programs for computing the composition of the solutions containing multiple metals and ligands used for experiments in skinned muscle cells. *J. Physiol. (Paris).* 75:463–505.

Ford, S.J., M. Chandra, R. Mamidi, W. Dong, and K.B. Campbell. 2010. Model representation of the nonlinear step response in cardiac muscle. *J. Gen. Physiol.* 136:159–177. https://doi.org/10.1085/jgp.201010467

Ford, S.J., R. Mamidi, J. Jimenez, J.C. Tardiff, and M. Chandra. 2012. Effects of R92 mutations in mouse cardiac troponin T are influenced by changes in myosin heavy chain isoform. *J. Mol. Cell. Cardiol.* 53:542–551. https://doi.org/10.1016/j.yjmcc.2012.07.018

Gollapudi, S.K., R. Mamidi, S.L. Mallampalli, and M. Chandra. 2012. The N-terminal extension of cardiac troponin T stabilizes the blocked state of cardiac thin filament. *Biophys. J.* 103:940–948. https://doi.org/10.1016/j.bpj.2012.07.035

Stienen, G.J., R. Zaremba, and G. Elzinga. 1995. ATP utilization for calcium uptake and force production in skinned muscle fibres of Xenopus laevis. *J. Physiol.* 482:109–122. https://doi.org/10.1113/jphysiol.1995.sp020503